metals

MDPI

Article

Internal Elastic Strains of AZ31B Plate during Unloading at Twinning-Active Region

Qichang He, Xiangyu Zhou, Xiaodan Zhang, Chuhao Liu and Huamiao Wang *

School of Mechanical Engineering, Shanghai Jiao Tong University, Shanghai 200240, China; heqc@sjtu.edu.cn (Q.H.); sjtuzhouxy@sjtu.edu.cn (X.Z.); 019020910126@sjtu.edu.cn (X.Z.); liuchuhao@sjtu.edu.cn (C.L.)

* Correspondence: wanghm02@sjtu.edu.cn; Tel.: +86-21-34206770

Abstract: Magnesium alloys, being the lightest structural metals, have garnered significant attention in various fields. The characterization of inelastic behavior has been extensively investigated by researchers due to its impact on structural component performance. However, the occurrence of twinning in the absence of any applied driving force during unloading has lacked reasonable explanations. Moreover, the influence of deformation mechanisms other than twinning on inelastic behavior remains unclear. In this study, uniaxial tension and compression tests were conducted on hot-rolled magnesium alloy plates, and neutron diffraction experiments were employed to characterize the evolution of macroscopic mechanical response and microscopic mechanisms. Additionally, a twinning and detwinning (TDT) model based on the elastic visco-plastic self-consistent (EVPSC) model has been proposed, incorporating back stress to describe the deformation behavior during stress relaxation. This approach provides a comprehensive understanding of the inelastic behavior of magnesium alloys from multiple perspectives and captures the influence of microscale mechanisms. A thorough understanding of the inelastic behavior of magnesium alloys and a reasonable explanation for the occurrence of twinning under zero-stress conditions offer valuable insights for the precise design of magnesium alloy structures.

Keywords: magnesium alloys; inelastic; crystal plasticity; twinning; detwinning; neutron diffraction

check for updates

Citation: He, Q.; Zhou, X.; Zhang, X.; Liu, C.; Wang, H. Internal Elastic Strains of AZ31B Plate during Unloading at Twinning-Active Region. *Metals* **2023**, *13*, 1388. https://doi.org/10.3390/met13081388

Academic Editor: Jiro Kitagawa

Received: 26 June 2023
Revised: 18 July 2023
Accepted: 27 July 2023
Published: 2 August 2023

Copyright: © 2023 by the authors. Licensee MDPI, Basel, Switzerland. This article is an open access article distributed under the terms and conditions of the Creative Commons Attribution (CC BY) license (https://creativecommons.org/licenses/by/4.0/).

1. Introduction

As the lightest structural metal, magnesium (Mg) alloys attract much attention in automotive, aerospace and electronics industries [1,2]. Extensive studies have been devoted to uncovering the underlying mechanisms related to deformation behavior affecting the design of magnesium alloy structural parts. One of the important characteristics for the accurate design of magnesium structural components is the inelastic behavior, which refers to the non-linear relationship between stress and strain during the unloading process [3–5]. This inelastic behavior has a significant impact on the key properties of magnesium alloy structures, for instance, damping coefficients, apparent elastic constants, spring back, and the fatigue property [6–8]. Plastic deformation of magnesium alloys is mainly accommodated by both slip and twinning at room temperature. De-twinning may take place upon loading reversal after twinning [9], which was also ascribed to be partially responsible for the inelastic behavior during unloading [10]. Noteworthy inelastic strains have been observed during unloading of Mg and its alloys [3,4,11]. Gharghouri et al. [11] ascribed the inelastic behavior to both deformation mechanisms of extension twin and slip mechanisms. Muránsky et al. [5] showed that the inelastic response of Mg alloy extruded bars is more pronounced under compressive unloading than tensile unloading due to detwinning by in-situ neutron diffraction techniques. Similar behaviors have been observed in pure Mg [12] and magnesium alloys [13,14].

While mechanical experiments are vital to understand the deformation mechanisms of inelastic behaviors, crystal plasticity (CP)-based simulations are of equal importance

to analyze the causes of inelastic behavior. The crystal plasticity theory connects the macroscopic inelastic behaviors to the deformation mechanisms at the scale of grains. The crystal plasticity finite element method (CPFEM), one of the full-field CP approaches, can be combined with a wide range of deformation mechanisms and was used in extensive magnesium alloy simulations [15–18]. Hama et al. [13,14] conducted a crystal plastic finite element analysis on the loading and unloading process of rolled magnesium alloy sheet under uniaxial tensile action and studied the inelastic response mechanism (the influence of substrate slip and non-substrate slip systems) during the unloading process of rolled magnesium alloy sheet. Due to its computational complexity, the wide applications of CPFEM simulations are limited by their high computational cost. Moreover, the challenge of parameter calibration brings obstacles to the application of CPFEM. Chang et al. [19] respectively simulated the inelastic behavior of magnesium with a detailed CPFEM model considering the full set of slip and twins and a reduced-order CPFEM model significantly simplifying the slip system, and they drew the conclusion that excellent computational accuracy and high computational efficiency can hardly be satisfied in one model.

In view of its high computational efficiency and the description of various deformation mechanisms, the elastic visco-plastic self-consistent (EVPSC) model proposed by Wang et al. [20] has been widely applied in simulation of HCP materials under homogeneous and inhomogeneous deformation [21–23]. Wang et al. [24] proposed a physics-based twinning and detwinning (TDT) model on the basis of an EVPSC model (EVPSC-TDT) and used the EVPSC-TDT model in the study of the deformation mechanism in HCP materials [24–26]. For instance, Wang et al. [27,28] applied the EVPSC-TDT model in the simulation of the inelastic behavior of Mg alloy rolled sheets and accurately predicted the inelastic behavior of AZ31B rolled sheets during unloading. Cheng et al. [29] compared three state-of-the-art crystal plasticity-based twinning models from the literature, namely the elastic visco-plastic self-consistent twinning-detwinning (EVPSC-TDT) model, crystal plasticity finite-element model based on an enhanced predominate twin reorientation approach (CPFE-ePTR), and the crystal plasticity finite-element model based on a "discrete twinning" approach (CPFE-DT), and they came to the conclusion that the EVPSC-TDT method showed the highest computational efficiency. Inelastic behavior became more pronounced when twinning was activated, and detwinning was identified as the dominant deformation mechanism during unloading in the case of compressing the extruded bars.

While the inelastic behavior of magnesium alloy has been extensively studied in the literature, there has been a lack of reasonable explanations for the phenomenon of detwinning processes occurring when the overall stress is completely unloaded, and the contributions of other deformation mechanisms to inelastic behavior have received less interest. Based on a brief review of the inelastic behavior of magnesium alloys and crystal plasticity simulations, this study conducted neutron diffraction experiments and crystal plasticity model simulations. The aim was to provide an explanation for the phenomenon of detwinning processes during the unloading process and to investigate the influence of other deformation mechanisms on the inelastic behavior of magnesium alloys.

2. The Crystal Plasticity Model

In order to study the inelastic behavior of Mg alloys under compression, back stress is incorporated into the EVPSC model. If the back stress is not considered, the shear rate for a slip system in the EVPSC model is expressed by:

$$\dot{\gamma}^{\alpha} = \dot{\gamma}_0 \left| \frac{\tau^{\alpha}}{\tau^{\alpha}_{cr}} \right|^{n} sgn(\tau^{\alpha}) \quad (1)$$

in terms of the reference shear rate $\dot{\gamma}_0$, the resolved shear stress (RSS) τ^α, the critical resolved shear stress (CRSS) τ^α_{cr}, and the strain rate sensitivity $\frac{1}{n}$. The strain rate ($\dot{\varepsilon}_{ij}$) is dependent on both the elastic and plastic deformation rate ($\dot{\varepsilon}^e_{ij}$ and $\dot{\varepsilon}^p_{ij}$) and is expressed by:

$$\dot{\varepsilon}_{ij} = \dot{\varepsilon}^e_{ij} + \dot{\varepsilon}^p_{ij} = M^e_{ijkl}\dot{\sigma}_{kl} + \sum_\alpha \dot{\gamma}^\alpha P^\alpha_{ij} \tag{2}$$

where M^e_{ijkl} is the elastic compliance, σ_{kl} is Gauchy stress, and $P^\alpha_{ij} = \left(s^\alpha_i n^\alpha_j + n^\alpha_i s^\alpha_j\right)$ is the Schmid tensor for a slip/twinning system α.

The hardening of the slip systems during deformation is described by the dislocation density hardening law [30,31]. The threshold stresses for a slip system contain three terms:

$$\tau_{cr} = \tau_0 + \tau_{for} + \tau_{sub} \tag{3}$$

where τ_0 and τ_{for} are the initial threshold stress and the effect from a statistical distribution of stored dislocations $\rho_{tot} = \sum_\alpha \rho^\alpha$, and the last term $\tau_{sub} = 0$ is the contribution from the stored dislocation density within organized substructure ρ_{sub}, because there is not much debris at a strain of 4%. The relationship between the second component τ_{for} and ρ_{tot} is given by the Taylor relation:

$$\tau = b\chi\mu\sqrt{\rho_{tot}} \tag{4}$$

with $\chi = 0.2$ being the dislocation interaction parameter. The dislocation evolution is comprised of both storage and annihilation:

$$\frac{d\rho}{d\gamma} = k_1\sqrt{\rho} - k_2\rho \tag{5}$$

where k_1 represents a rate-insensitive factor that characterizes dislocation storage through statistical trapping of gliding dislocations by forest obstacles, and k_2 corresponds to a rate-sensitive factor associated with dynamic recovery, expressed by:

$$\frac{k_2\left(\dot{\varepsilon}, T\right)}{k_1} = \frac{\chi b}{g}\left(1 - \frac{kT}{Db^3} ln\left(\frac{\dot{\varepsilon}}{\dot{\varepsilon}_0}\right)\right) \tag{6}$$

where k, $\dot{\varepsilon}_0$, g, and D represent Boltzman's constant with a value of $1.38 \times 10^{-29}\left(\mathrm{MPa{\cdot}m^3/K}\right)$, a reference strain rate (10^7/s), a normalized effective activation enthalpy, and a drag stress, respectively. The hardening model assumes that as the population of slip dislocations increases, the threshold stress for twinning rises accordingly:

$$\tau^\beta_c = \tau^\beta_0 + \tau^\beta_{slip} = \tau^\beta_0 + \mu\sum_\alpha C^{\beta\alpha} b^\beta b^\alpha \rho^\alpha \tag{7}$$

where b^β is the magnitude of the Burgers vector for the twinning dislocation, and $C^{\beta\alpha}$ represents the coefficient that inhibits the growth of twinning system β due to the accumulation of dislocations from slip system α. The specific values of $C^{\beta\alpha}$ have minimal impact on the predicted outcomes, suggesting that the observed behavior is hardly affected by the coupling term in Equation (7).

The TDT model was used in conjunction with the EVPSC model, and four distinct operations were incorporated to describe the deformation processes associated with twinning and detwinning. For a more comprehensive understanding of the TDT model, further details can be found in the works of Wang et al. [23,24]. As we know, twinning will cause large local shear, which will cause large back stress in the parent grains, especially at the early stage of twinning. Therefore, it is necessary to account for the back stress, which is related to the shear strain caused by twinning. Therefore, we proposed the back stress as:

$$\sigma^{B,\alpha}_{ij} = -C_{ijkl} f^\alpha \gamma^T P^\alpha_{kl} \tag{8}$$

with f^{α} being the twin volume fraction of twinning system α, and γ^{T} the characteristic twinning shear (0.129 for Mg alloys). Therefore, the Cauchy stress in the parent crystal is corrected to:

$$\sigma_{ij}^{parent} = \frac{\sigma_{ij}^{parent} + \sum_{\alpha} f^{\alpha} \sigma_{ij}^{B,\alpha}}{1 - \sum_{\alpha} f^{\alpha}} \tag{9}$$

This correction reflects the back stress induced by the local twinning shear at the early stage of twinning.

3. Experiment Procedure

The studied material is a 25.4 mm thick hot-rolled AZ31B plate in the soft annealed condition (O temper) with an average grain size of 50 μm, and the initial texture was measured by the high-intensity pressure and preferred orientation (HIPPO) instrument. Different samples were machined from this plate and used in two different tests. The flat dog-bone-shaped tension sample with a rectangular gauge section (44 mm in length, 6.35 mm in height, and 5 mm in thickness) was used to uniaxial tension. The cylinder compression sample (diameter of 10 mm and a length of 24 mm) was used to uniaxial compression and compression with multiple unloadings. The loading direction aligns with the transverse direction (TD) of the rolled plate. During the experiment, an in situ compressive test was conducted with unloadings, and neutron diffraction data were collected during the loadings. The stress-strain curves for continuous tension and compression and the {00.1} pole figures of the discretized initial texture used for the simulations can be seen in Figure 1, while Figure 2a illustrates the stress–strain curves for the test with unloadings. The pole figures show that the as-received AZ31 plate had a very strong texture, evidenced by the strong {00.1} intensity along the plate normal direction (ND). The experimental setup involves a servo-hydraulic load frame positioned at a 45° angle to the incident beam. This orientation allows for the simultaneous measurement of diffraction patterns using a detector bank situated at 90° relative to the incident beam. The detector bank enables the measurement of diffraction patterns with scattering vectors parallel to the loading axis. The complete diffraction patterns in each detector bank are captured by time-of-flight technique. This technique allows for comprehensive characterization of the material's crystal structure and phase information during the experiment. Elastic lattice strains are calculated by analyzing the changes in peak position in the diffraction patterns during deformation through the equation $\varepsilon^{hk.l} = \left(d^{hk.l} - d_0^{hk.l}\right)/d_0^{hk.l}$, where $\varepsilon^{hk.l}$ represents the elastic lattice strain for a specific peak, $d^{hk.l}$ is the measured lattice spacing during deformation, and $d_0^{hk.l}$ is the stress-free reference lattice spacing corresponding to the same peak measured before applying any load to the sample. For a more comprehensive understanding of the experimental procedure, the study by Wang et al. [32] can be referred to.

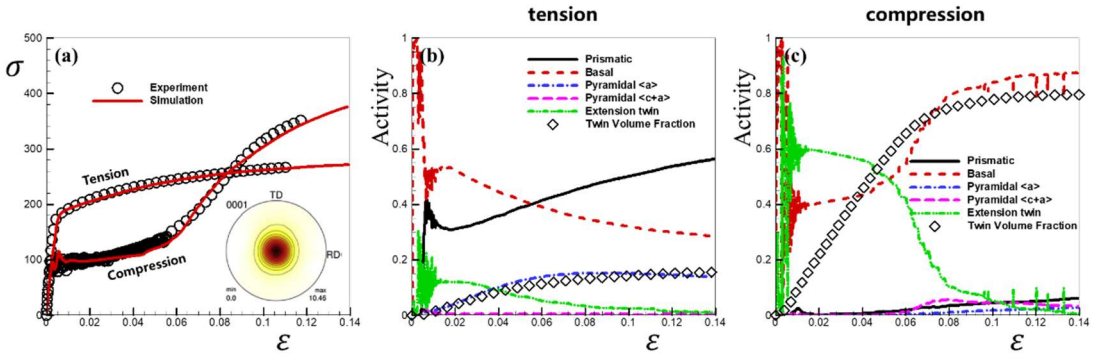


Figure 1. (**a**) Measured and predicted stress strain curves of AZ31 plate under uniaxial tension and compression. The initial texture of AZ31 is included. (**b**,**c**) The relative activities of deformation mechanisms and the twin volume fractions as functions of strain under tension and compression.

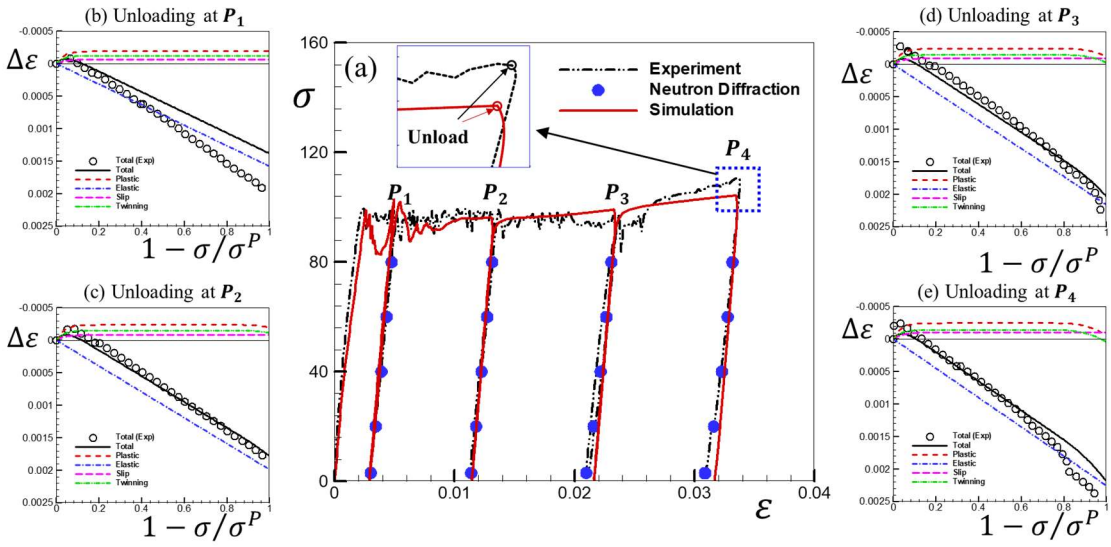


Figure 2. (**a**) Measured and predicted stress strain curves of AZ31 plate under compression with unloadings for neutron diffraction observation. (**b**–**e**) Total strain, elastic strain, plastic strain, plastic strains caused by twining and slip during each unloading. The vertical axis represents strain, which is marked as the variation in strain. The horizontal axis represents the unloading process, and the point $\left(1-\sigma/\sigma^P\right)$ = 0.2 represents the first of the five neutron diffraction measurement points during each unloading, while the point $\left(1-\sigma/\sigma^P\right)$ = 1 represents the neutron diffraction measurement point at complete stress unloading, and so on.

4. Results and Discussion

4.1. Parameter Calibration

The EVPSC-TDT model was applied to AZ31B plate, which is capable of interpreting the mechanical behavior of magnesium alloys [20–29,32–34]. The microstructure of the undeformed sample was measured and included in Figure 1a in terms of the {00.1} pole figure, which shows that the as-received AZ31 plate had extreme typical rolled texture [35,36]. The initial texture used in the model simulations is derived from the experimental orientation distribution function. The orientation distribution of the grains is discretized into 2160 grain orientations and used for simulations. Basal slip $(\{0001\}\langle 11\bar{2}0\rangle)$, prismatic $\langle a\rangle$ slip $(\{10\bar{1}0\}\langle 11\bar{2}0\rangle)$, pyramidal $\langle c+a\rangle$ slip $(\{10\bar{1}0\}\langle 11\bar{2}0\rangle)$ systems, and $\{10\bar{1}2\}\langle\bar{1}011\rangle$ extension twinning systems are the mechanisms considered in the modelling to accommodate plastic deformation [20,37,38]. At room temperature, the elastic constants of the magnesium alloy are: C_{11} = 58, C_{12} = 25, C_{13} = 20.8, C_{33} = 61.2, and C_{44} = 16.6 (GPa) [39]. As listed in Table 1, the model parameters were calibrated by fitting the stress–strain curves of continuous tension and compression, as illustrated in Figure 1a with a decent consistency. In addition, the relative activity of various deformation mechanisms and the twin volume fraction of extended twins predicted by the EVPSC-TDT model are shown in Figure 1b,c. The main deformation mechanism under tension is basal and prismatic slips, while twinning is suppressed. However, in the case of compression, extension twins are intensively activated, and twinning and basal slip serve as the primary deformation mechanisms. In the studied texture, the prismatic slip during compression exhibits a lower resolved shear stress (RSS) compared to the critical resolved shear stress (CRSS). Conversely, twinning has a higher resolved shear stress than the critical resolved shear stress (CRSS), and compression conditions favor the activation of twinning. Additionally, the saturated volume fraction of twins exhibits a significant increase compared to the loading condition under tension. Twinning dominates the deformation up to a strain of 0.055 under compression. Beyond that, basal slip takes over as the dominant mechanism, while other slip systems supplement the plastic deformation. When the strain reaches 0.08, twinning becomes saturated, and the twinning relative activity becomes significantly reduced.

Table 1. List of values of the parameters involved in the EVPSC-TDT model.

Mode	τ_0 (MPa)	ρ_0^α (m^{-2})	b^α (Å)	k_1 (m)	g^α	D^α (MPa)	$C^{\alpha\beta}$	χ	n
Basal	98	1×10^7	3.21	8×10^9	0.033	80	1	0.2	13
Prismatic	25	1×10^7	3.21	4×10^8	0.033	80	1	0.2	13
Pyramidal	315	1×10^7	6.12	1.2×10^8	0.033	80	1	0.2	13
Twinning	35	NA *	0.492	NA	NA	NA	NA	NA	13

* NA: not applicable.

4.2. Mechanical Behaviors during Cyclic Loading-Unloading

In the unloading test, the stress was unloaded at the strains of 0.03, 0.01, 0.02, and 0.03, where neutron diffraction data were collected at five stresses in each unloading. The EVPSC-TDT model considering the twin-induced back stress captures well the stress–strain response during both the loading and unloading stages. The typical plateau of the stress as a function of the strain during loading is observed, which corresponds to a twinning-active loading region. The simulation curve in Figure 2a displays an uneven trend due to the influence of early fluctuations in the deformation mechanisms. The stress levels at unloading points during the four unloadings in the simulation are relatively consistent, whereas in the experiment, the stress at point P4 is noticeably higher than the preceding three points. Overall, the simulated curve shows good correspondence with the experimental curve. The experimental and predicted total strain during the compressive unloading are shown in Figure 2b–e, where reasonable agreement is obtained. Especially, given that the magnitude of the vertical axis is in the order of 10^{-3}, the measured increase in total strain at the early stage of each unloading is well reproduced by the simulations (Figure 2b–e). During the unloading process, the deviation between the simulation and experimental data was not more than 22% when the unloading reached 0.4. This deviation decreased with the increase in loading–unloading cycles and reached 9% and 2% for the third and fourth unloading, respectively. Achieving accurate data correspondence at this level of magnitude (10^{-3}) is a highly challenging task, particularly for the first unloading process. Since the elastic strain decreases monotonically during unloading, the increase in total strain has to be attributed to the plastic deformation of the Mg alloys. Towards the end of the unloading phase, pronounced inelastic behavior led by the change in the magnitude of plastic strain increment was observed. Slip systems and twinning systems are the deformation mechanisms considered to accommodate plastic deformation, and plastic strain caused by twinning contributes to the main portion of the plastic deformation during the unloading process.

The experimental and predicted internal elastic strains' change in different grain subsets during unloading are compared in Figure 3. The discrepancies observed in the simulation results of Figure 3 are attributed to the interactions between grain boundaries, which manifest as residual lattice elastic strain in the experiments. However, the omission of grain boundary interactions in the model lead to inaccuracy in the simulation results. As the loading–unloading cycles progress, a sufficient number of twins allows the detwinning behavior to effectively release the residual lattice elastic strain, leading to improved agreement between the simulation results and experimental observations. Additionally, it is worth noting that the strain magnitudes are in the order of 10^{-3}, a very small scale. Achieving precise correspondence between simulation and experimental results at such a small scale is challenging, but we have successfully captured the overall trend of the data. Both the experimental and predicted internal elastic strains decrease within all the grain subsets during unloading. The {11.0} grain subset exhibits the highest internal elastic strains. This is because the {11.0} subset is hard grain orientations and the {00.2} subset is relatively compliant, while the {10.1} and {10.3} subsets are intermediate. The {00.2} grain subset is oriented favorably for the activation of extension twin. Although lattice strains are typically elastic, the nonlinear curve shape of the {00.2} grain subset shows inelastic behavior at the end of unloading related to extension twin. The occurrence of inelastic

behavior suggests the redistribution of stress among different grain subsets. The deviation between the simulation and test curves of the {00.2} grain subsets ({10.3} as well) during unloading reflects the fact that twins are localized initially, but the internal elastic strain predicted by the EVPSC-TDT model is statistical. With increasing the loaded strain, the twins grow, and the predicted results conform more and more to the experiments.

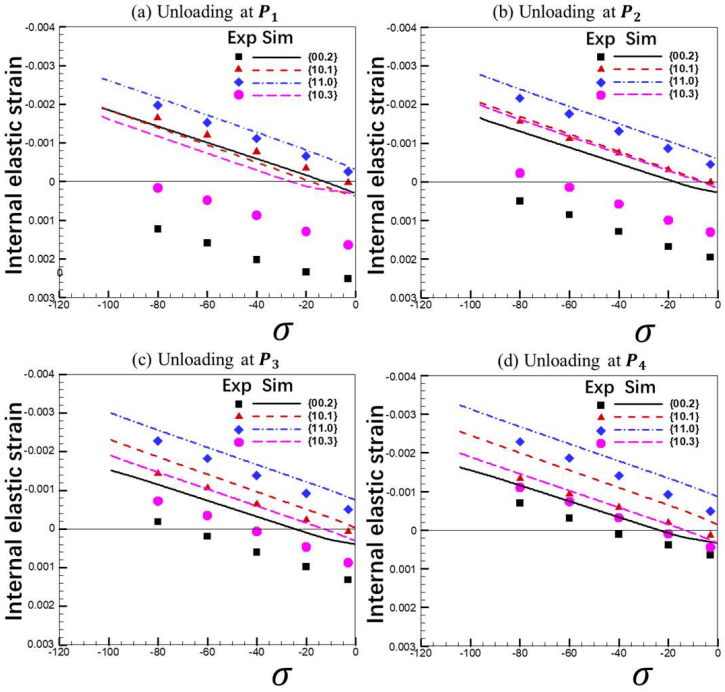


Figure 3. Internal elastic strains of {00.2}, {10.1}, {11.0}, and {10.3} grain subsets as a function of applied stress (σ) during each compression unloading. The horizontal axis represents the stress during unloading process.

In order to further reveal the deformation mechanisms of inelastic behavior, Figure 4 shows the normalized diffraction intensities of the {00.2} grain subset, the relative activities of various deformation mechanisms, and the twin volume fraction at the four unloadings. Due to the advantage of our model, we are able to conduct quantitative analyses on specific microstructural features. The relative diffraction intensities are normalized by 28, 53, 81 and 144, respectively, indicating an overall increase in the diffraction intensity with the loaded strain due to twinning. Upon complete unloading, the corresponding reductions in the relative diffraction intensities are 1.68, 2.65, 2.43, and 2.88, respectively. During the unloading process, the plateaus of twin volume fraction are determined to be 0.037, 0.147, 0.272, and 0.392, respectively. Upon complete unloading, the corresponding reductions in the twin volume fractions are 0.002, 0.005, 0.005, and 0.006, respectively. The simulated results of the {00.2} diffraction intensity at the five neutron diffraction measurement points during each loading–unloading cycle exhibit a deviation of less than 2% when compared to the experimental data. The simulation results reproduce the diffraction intensity of the {00.2} grain subset well. Both the increase in the intensity at the beginning of unloading and the decrease at the end are reproduced by the EVPSC-TDT model. The diffraction intensity of the {00.2} grain subset is closely related to the twinning activity. The increase in intensity of the {00.2} grain subset corresponds to twinning, as does the decrease to detwinning. The EVPSC-TDT model accounting for the back stress captures reasonably the inelastic behavior during unloading. The twinning and detwinning activity can also be reflected by the twinning activity and the twin volume fraction given by the model (the symbols in lower figures). We can clearly see the initial increase and final decrease in the twin volume fraction during unloadings. As shown in Figure 4b–d, noticeable increase in

twinning activity and decrease in basal slip activity are followed by re-establishment of twinning as the dominant mechanism towards the end of unloading. During this period, a simultaneous decrease in the volume fraction of twinning suggests the occurrence of detwinning behavior. The previously formed twins are de-twinned, which is in the same sense reflected by the decrease in the diffracted intensities {00.2}. The accumulation of twinning leads to an earlier occurrence of detwinning, which is consistent with the trend of {00.2} diffraction intensity up to zero. However, the phenomenon that the detwinning process occurs even when the stress is unloaded to zero means that the detwinning are not solely dependent on the applied stress. This is reasonable because, despite the absence of external stress, the internal elastic strains of the {10.3} and {00.2} grain subsets with opposite signs due to back stress are observed in Figure 3, and the resulting internal stress leads to the persistence of detwinning. Moreover, the impact of back stress varies across the four loading–unloading cycles, and the model effectively captures this behavior. It is important to note that the texture under investigation exhibits a high propensity for twin formation, and it is expected that in other randomly textured materials, the reduction in twin volume fraction due to back stress is not significant.

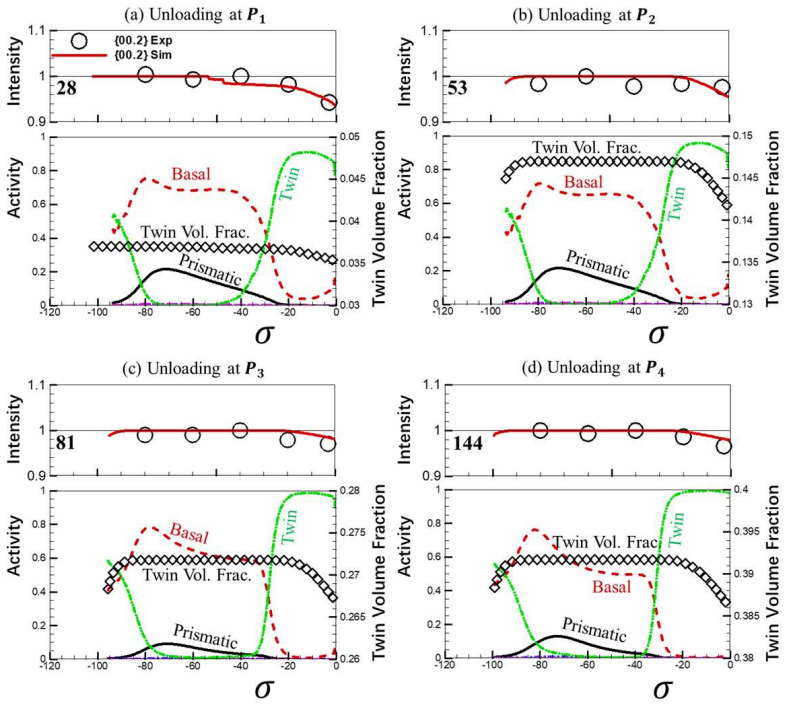


Figure 4. Measured and predicted diffraction intensity of the {00.2} grain subset, predicted relative activity of various deformation mechanisms, and twin volume fraction as a function of applied stress (σ) during each compression unloading. The abscissa of the intensity corresponds to the activity and twin volume fraction.

5. Concluding Remarks

The primary objective of this study was to gain a comprehensive understanding of the mechanical behavior exhibited by AZ31B magnesium alloy during uniaxial compression, specifically focusing on the unloading phase. To achieve this objective, a combination of in situ neutron diffraction measurements and the EVPSC-TDT model incorporating back stress effects was employed. Based on the obtained results, the following conclusions can be drawn:

1. Magnesium alloys exhibit significant inelastic behavior during the unloading, and this phenomenon was observed consistently in both modeling and experimental studies.
2. In situ neutron diffraction experiments have captured the decrease in {00.2} diffraction intensity and the evolution of lattice strains during stress relaxation. The residual

lattice elastic strain can be released spontaneously by detwinning behavior if the twins are sufficient. Prior to the stress unloading reaching zero, the internal elastic strains of the {00.2} and {10.3} planes have already decreased to zero and exhibited strains with opposite signs due to twin-induced back stress. This leads to the development of internal stresses within the material, triggering the activation of detwinning processes. The quantity of twins has a significant impact on the effectiveness of back stress; as the twin volume fraction increases, the impact of back stress becomes more pronounced.

3. The EVPSC-TDT model, incorporating back stresses, exhibits excellent predictive capabilities for the macroscopic stress–strain response and evolution of diffraction intensities, demonstrating excellent agreement with experimental measurements. Given that the magnitude of the vertical axis is in the order of 10^{-3}, the deviation between the simulation and experimental data is less than 20% when the unloading reached 0.4. The model effectively captures the reduction in twin volume fraction with a deviation less than 2% and provides a reasonable explanation for the discrepancies observed in simulated microscale lattice elastic strains. Furthermore, the model elucidates that the inelastic behavior of magnesium alloys is closely associated with significant detwinning and basal slip activities.
4. Under tensile loading, the predominant deformation mechanisms in magnesium alloys are basal slip and prismatic slip. Conversely, under compression, twinning is prominently activated and becomes a dominant deformation mechanism alongside basal slip. In addition to detwinning, basal slip is also a responsible deformation mechanism for inelastic behavior, and prismatic slip complements the inelastic behavior.

The findings from this study contribute to advancing our knowledge of the mechanical response of AZ31B magnesium alloy under uniaxial compression with unloadings. The insights gained from this research can aid in the development of more accurate predictive models and assist in the design and optimization of magnesium alloy-based structural components for various engineering applications.

Author Contributions: Conceptualization, Q.H. and H.W.; methodology, H.W.; validation, Q.H. and H.W.; formal analysis, Q.H.; investigation, X.Z. (Xiangyu Zhou); resources, Q.H.; data curation, H.W.; writing—original draft preparation, X.Z. (Xiangyu Zhou) and C.L.; writing—review and editing, X.Z. (Xiangyu Zhou), H.W., C.L. and X.Z. (Xiaodan Zhang); visualization, H.W. and C.L.; supervision, H.W.; project administration, Q.H. and H.W. All authors have read and agreed to the published version of the manuscript.

Funding: This research received no external funding.

Data Availability Statement: The data that support the findings of this study are available from the corresponding author upon reasonable request.

Conflicts of Interest: The authors declare no conflict of interest.

References

1. Song, J.; Chen, J.; Xiong, X.; Peng, X.; Chen, D.; Pan, F. Research Advances of Magnesium and Magnesium Alloys Worldwide in 2021. *J. Magnes. Alloy* **2022**, *10*, 863–898. [CrossRef]
2. Prasad, S.V.S.; Prasad, S.B.; Verma, K.; Mishra, R.K.; Kumar, V.; Singh, S. The Role and Significance of Magnesium in Modern Day Research-A Review. *J. Magnes. Alloy* **2022**, *10*, 1–61. [CrossRef]
3. Zhu, G.; Yang, C.; Shen, G.; Peng, Y.; Shi, B. The Asymmetric Pre-Yielding Behaviour during Tension and Compression for a Rolled AZ31 Mg Alloy. *Int. J. Mater. Form.* **2022**, *15*, 26. [CrossRef]
4. Bong, H.J.; Lee, J.; Lee, M.-G. Modeling Crystal Plasticity with an Enhanced Twinning–Detwinning Model to Simulate Cyclic Behavior of AZ31B Magnesium Alloy at Various Temperatures. *Int. J. Plast.* **2022**, *150*, 103190. [CrossRef]
5. Muránsky, O.; Carr, D.G.; Šittner, P.; Oliver, E.C. In situ neutron diffraction investigation of deformation twinning and pseudoelastic-like behaviour of extruded AZ31 magnesium alloy. *Int. J. Plast.* **2009**, *25*, 1107–1127. [CrossRef]
6. Tang, W.; Lee, J.Y.; Wang, H.; Steglich, D.; Li, D.; Peng, Y.; Wu, P. Unloading Behaviors of the Rare-Earth Magnesium Alloy ZE10 Sheet. *J. Magnes. Alloy* **2021**, *9*, 927–936. [CrossRef]
7. Wagoner, R.H.; Lim, H.; Lee, M.-G. Advanced issues in springback. *Int. J. Plast.* **2013**, *45*, 3–20. [CrossRef]
8. Ling, Y.; Roostaei, A.A.; Glinka, G.; Jahed, H. Fatigue of ZEK100-F magnesium alloy: Characterisation and modelling. *Int. J. Fatigue* **2019**, *125*, 179–186. [CrossRef]

9. Lou, X.Y.; Li, M.; Boger, R.K.; Agnew, S.R.; Wagoner, R.H. Hardening evolution of AZ31B Mg sheet. *Int. J. Plast.* **2007**, *23*, 44–86. [CrossRef]
10. Wang, H.; Wu, P.D.; Wang, J. Modeling inelastic behavior of magnesium alloys during cyclic loading–unloading. *Int. J. Plast.* **2013**, *47*, 49–64. [CrossRef]
11. Gharghouri, M.A.; Weatherly, G.C.; Embury, J.D.; Root, J. Study of the mechanical properties of Mg-7.7at.% Al by in-situ neutron diffraction. *Philos. Mag. A* **1999**, *79*, 1671–1695. [CrossRef]
12. Li, Y.; Enoki, M. Recovery behaviour of pure magnesium in cyclic compression–quick unloading-recovery process at room temperature investigated by AE. *Mater. Trans.* **2008**, *49*, 1800–1805. [CrossRef]
13. Hama, T.; Takuda, H. Crystal-plasticity finite-element analysis of inelastic behavior during unloading in a magnesium alloy sheet. *Int. J. Plast.* **2011**, *27*, 1072–1092. [CrossRef]
14. Hama, T.; Kitamura, N.; Takuda, H. Effect of twinning and detwinning on inelastic behavior during unloading in a magnesium alloy sheet. *Mater. Sci. Eng. A* **2013**, *583*, 232–241. [CrossRef]
15. Yaghoobi, M.; Chen, Z.; Murphy-Leonard, A.D.; Sundararaghavan, V.; Daly, S.; Allison, J.E. Deformation Twinning and Detwinning in Extruded Mg-4Al: In-Situ Experiment and Crystal Plasticity Simulation. *Int. J. Plast.* **2022**, *155*, 103345. [CrossRef]
16. Huang, W.; Chen, J.; Zhang, R.; Yang, X.; Jiang, L.; Xiao, Z.; Liu, Y. Effect of deformation modes on continuous dynamic recrystallization of extruded AZ31 Mg alloy. *J. Alloy Compd.* **2022**, *897*, 163086. [CrossRef]
17. Frydrych, K.; Libura, T.; Kowalewski, Z.; Maj, M.; Kowalczyk-Gajewska, K. On the Role of Slip, Twinning and Detwinning in Magnesium Alloy AZ31B Sheet. *Mater. Sci. Eng. A* **2021**, *813*, 141152. [CrossRef]
18. Bong, H.J.; Hu, X.; Sun, X.; Ren, Y. Temperature-Dependent Constitutive Modeling of a Magnesium Alloy ZEK100 Sheet Using Crystal Plasticity Models Combined with in Situ High-Energy X-Ray Diffraction Experiment. *J. Magnes. Alloy* **2022**, *10*, 2801–2816. [CrossRef]
19. Chang, Y.; Lloyd, J.T.; Becker, R.; Kochmann, D.M. Modeling microstructure evolution in magnesium: Comparison of detailed and reduced-order kinematic models. *Mech. Mater.* **2017**, *108*, 40–57. [CrossRef]
20. Wang, H.; Wu, P.D.; Tomé, C.N.; Huang, Y. A finite strain elastic–viscoplastic self-consistent model for polycrystalline materials. *J. Mech. Phys. Solids* **2010**, *58*, 594–612. [CrossRef]
21. Wang, F.H.; Qiao, H.; Wang, Y.Q.; Dong, J.; Jiang, Y.Y.; Wu, P.D. Numerical Study of Deformation Behavior of Rolled AZ31B Plate under Cyclic Loading in Different Material Orientations Based on the EVPSC-TDT Model. *Int. J. Plast.* **2021**, *147*, 103109. [CrossRef]
22. Tang, D.; Zhou, K.; Tang, W.; Wu, P.; Wang, H. On the Inhomogeneous Deformation Behavior of Magnesium Alloy Beam Subjected to Bending. *Int. J. Plast.* **2022**, *150*, 103180. [CrossRef]
23. Zhang, X.; Li, S.; Guo, X.; Wang, H.; Yu, Q.; Wu, P. Effects of Texture and Twinning on the Torsional Behavior of Magnesium Alloy Solid Rod: A Crystal Plasticity Approach in Comparison with Uniaxial Tension/Compression. *Int. J. Mech. Sci.* **2021**, *191*, 106062. [CrossRef]
24. Wang, H.; Wu, P.D.; Wang, J.; Tomé, C.N. A crystal plasticity model for hexagonal close packed (HCP) crystals including twinning and de-twinning mechanisms. *Int. J. Plast.* **2013**, *49*, 36–52. [CrossRef]
25. Wang, H.; Wu, P.D.; Wang, J. Modelling the role of slips and twins in magnesium alloys under cyclic shear. *Comp. Mater. Sci.* **2015**, *96*, 214–218. [CrossRef]
26. Wang, H.; Wu, P.; Kurukuri, S.; Worswick, M.J.; Peng, Y.; Tang, D.; Li, D. Strain rate sensitivities of deformation mechanisms in magnesium alloys. *Int. J. Plast.* **2018**, *107*, 207–222. [CrossRef]
27. Wang, H.; Tang, D.; Li, D.Y.; Peng, Y.H.; Wu, P.D. Effects of detwinning on the inelasticity of AZ31B sheets during cyclic loading and unloading. *Int. J. Appl. Mech.* **2018**, *10*, 1850095. [CrossRef]
28. Wang, H.; Li, D.; Peng, Y.; Wu, P.D. Numerical study of inelastic behavior of magnesium alloy sheets during cyclic loading-unloading. *J. Phys. Conf. Ser.* **2018**, *1063*, 012050. [CrossRef]
29. Cheng, J.; Jong Bong, H.; Qiao, H.; Hu, X.; Sun, X.; Ghosh, S.; Wu, P. Comparison of Three State-of-the-Art Crystal Plasticity Based Deformation Twinning Models for Magnesium Alloys. *Comput. Mater. Sci.* **2022**, *210*, 111480. [CrossRef]
30. Beyerlein, I.J.; Tomé, C.N. A dislocation-based constitutive law for pure Zr including temperature effects. *Int. J. Plast.* **2008**, *24*, 867–895. [CrossRef]
31. Capolungo, L.; Marshall, P.E.; McCabe, R.J.; Beyerlein, I.J.; Tomé, C.N. Nucleation and growth of twins in Zr: A statistical study. *Acta Mater.* **2009**, *57*, 6047–6056. [CrossRef]
32. Wang, H.; Clausen, B.; Capolungo, L.; Beyerlein, I.J.; Wang, J.; Tomé, C.N. Stress and strain relaxation in magnesium AZ31 rolled plate: In-situ neutron measurement and elastic viscoplastic polycrystal modeling. *Int. J. Plast.* **2016**, *79*, 275–292. [CrossRef]
33. Wang, H.; Clausen, B.; Tomé, C.N.; Wu, P.D. Studying the effect of stress relaxation and creep on lattice strain evolution of stainless steel under tension. *Acta Mater.* **2013**, *61*, 1179–1188. [CrossRef]
34. Wang, H.; Wu, P.; Wang, J. Numerical assessment of the role of slip and twinning in magnesium alloy AZ31B during loading path reversal. *Metall. Mater. Trans. A* **2015**, *46*, 3079–3090. [CrossRef]
35. Proust, G.; Tomé, C.N.; Jain, A.; Agnew, S.R. Modeling the effect of twinning and detwinning during strain-path changes of magnesium alloy AZ31. *Int. J. Plast.* **2009**, *25*, 861–880. [CrossRef]

36. Wu, L.; Agnew, S.R.; Ren, Y.; Brown, D.W.; Clausen, B.; Stoica, G.M.; Wenk, H.R.; Liaw, P.K. The effects of texture and extension twinning on the low-cycle fatigue behavior of a rolled magnesium alloy, AZ31B. *Mater. Sci. Eng. A* **2010**, *527*, 7057–7067. [CrossRef]
37. Agnew, S.R.; Duygulu, Ö. Plastic anisotropy and the role of non-basal slip in magnesium alloy AZ31B. *Int. J. Plast.* **2005**, *21*, 1161–1193. [CrossRef]
38. Jain, A.; Agnew, S.R. Modeling the temperature dependent effect of twinning on the behavior of magnesium alloy AZ31B sheet. *Mater. Sci. Eng. A* **2007**, *462*, 29–36. [CrossRef]
39. Simmons, G.; Wang, H. *Single Crystal Elastic Constants and Calculated Aggregate Properties: A Handbook*, 2nd ed.; M.I.T. Press: Cambridge, MA, USA, 1971; ISBN 978-0-262-19092-3.

Disclaimer/Publisher's Note: The statements, opinions and data contained in all publications are solely those of the individual author(s) and contributor(s) and not of MDPI and/or the editor(s). MDPI and/or the editor(s) disclaim responsibility for any injury to people or property resulting from any ideas, methods, instructions or products referred to in the content.